M&C 2017 - International Conference on Mathematics & Computational Methods Applied to Nuclear Science & Engineering, Jeju, Korea, April 16-20, 2017, on USB (2017)

Generalised Boltzmann Fokker-Planck Elastic Scattering using the Evaluated Electron Data Library

Daniel M. Fletcher*, Brian C. Franke†

*AWE Plc. Aldermaston, Reading, Berkshire RG7 4PR, UK
†Sandia National Laboratories, P.O. Box 5800, Albuquerque, NM 87185-1179
daniel.fletcher@awe.co.uk, bcfrank@sandia.gov

Abstract - *The coupled electron-photon Monte Carlo transport code ITS (Integrated Tiger Series) has recently been extended to include a single-scattering algorithm using data from the evaluated cross section data libraries from LLNL (Lawrence Livermore National Laboratories) to enable transport below 1 keV. In order to begin improving the computational efficiency of this algorithm, a moment preserving modification to the electron elastic scattering cross sections known as the GBFP (Generalised Boltzmann Fokker-Planck) method has been implemented and is described here. The method is then applied to a variety of test problems, where it is seen to be in good agreement with experimental and analogue Monte Carlo results, while significantly decreasing the processing required for elastic scattering. However, the runtimes are still limited by inelastic processes, and the method must be extended to include these to observe a significant improvement in runtime.*

I. INTRODUCTION

Recent development efforts on the Integrated Tiger Series (ITS)[1] Code have worked towards implementing photon and electron transport using cross sections and data provided in the EEDL (Evaluated Electron Data Library), EPDL (Evaluated Photon Data Library) and EADL (Evaluated Atomic Data Library)[2] developed at LLNL to extend transport below 1 keV. To take advantage of the detailed atomic data available, a single-scattering algorithm has been developed.

The analogue Monte Carlo transport of electrons is however computationally intensive due to the short mean free paths associated with long range Coulomb interactions. These interactions lead to a differential cross section which is highly peaked in the forward direction. The generalised Boltzmann Fokker-Planck (GBFP) method[3, 4] (or Moment-Preserving method) aims to replace a portion of the tabulated differential cross section (DCS) with an approximate DCS based on discrete angles. By preserving only a finite number of differential cross section moments, the GBFP method is computationally efficient, and has been shown to be accurate and robust for a wide range of physics, including stochastic media problems[5]. In this paper, the GBFP method is applied using the electron elastic scattering data contained in the EEDL. The accuracy and efficiency of the GBFP method are assessed mostly relative to analogue simulations. As this is the first publication assessing the performance of the single-scattering algorithm in ITS based on the LLNL data libraries, comparisons are also made with experimental data and the traditional condensed history algorithm in ITS.

II. THEORY

For elastic scattering, the EEDL provides a table of the total cross section on an energy grid between 10 eV and 100 GeV. The distance to a collision for an electron with energy E is obtained by using an interpolated value of the tabulated total cross section, $\sigma_{elast}(E)$. A much coarser energy grid structure is used to tabulate scattering angles and their corresponding probability. The tabulated data however does not cover the full range of $\mu = \cos\theta$ scattering angles, instead just the range from $\mu = -1$ to $\mu = \mu_{sr} = 1 - 10^{-6}$. This is due to angular distributions becoming increasingly forward peaked and difficult to resolve on a grid with increasing energy. Instead, an analytical function $f(\mu) = A/(\eta + 1 - \mu)^2$ is prescribed for the angular probabilities above μ_{sr}, where A is a normalising factor to ensure continuity with the tabulated data at μ_{sr} and η is the screening parameter due to Seltzer[6].

The essence of the GBFP method is to replace the tabulated $\sigma(\mu, E)$ differential cross section with an approximate cross section, $\tilde{\sigma}(\mu, E)$ represented as a superposition of discrete scattering angles,

$$\tilde{\sigma}(\mu, E) = \sum_{l=1}^{L} \frac{\alpha_l(E)}{2\pi} \delta\left[\mu - \xi_l(E)\right] + \frac{\alpha_0(E)}{2\pi}\delta[\mu - 1] \qquad (1)$$

which is constrained to conserve a finite number of momentum transfer moments,

$$\sigma_{n,elast}(E) = \tilde{\sigma}_{n,elast}(E) \quad n = 0, 1, 2... 2L \qquad (2)$$

where the momentum transfer moments are given by

$$\sigma_{n,elast}(E) = 2\pi \int_{-1}^{1} (1-\mu)^n \sigma(\mu, E) d\mu \quad n = 0, 1, 2... \qquad (3)$$

An eight point Gauss-Legendre quadrature is used to calculate the moments of the EEDL tabulated differential cross section, where the data is interpolated to the quadrature points using the method suggested in the EEDL data file piecewise across each angular bin. A recursion relation[7] is used for the moments of the analytic portion above μ_{sr}, as the quadrature becomes increasingly poor at capturing the forward peak at higher energies. Equation 2 represents a nonlinear system of equations for the discrete scattering angles, ξ_l and corresponding amplitudes α_l that is solved using a method developed by Sloan et al.[8, 9]. Sloan's method utilises a Radau quadrature which ensures that an angle will be generated in the forward direction. The amplitude of this angle can then be removed from the interaction cross section, and thus the distance to

interaction is increased. In electron transport calculations, the mean free paths are short compared to geometry features. The computational cost is dominated by the processing of interactions. Reducing the number of interactions in the simulation can speed up the simulation proportionally. While all interaction types need to be considered, here we consider only the elastic scattering interaction, which dominates at high energies. From Figure 1, we see that the GBFP method reduces the elastic interaction cross section by factor between 10 and 100 at 100 keV, by about a factor of 100 to 1000 at 10 MeV, and by several orders of magnitude at 1 GeV. In the results, we focus on lower energies where analogue simulations are computationally affordable. However, the greatest benefit of the method is at higher energies.

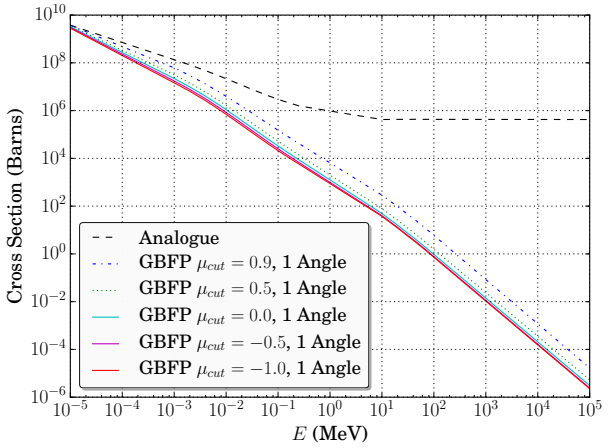

Fig. 1: Reduction in the electron elastic cross section in silicon for decreasing μ_{cut}

1. Hybrid Method

A hybrid method[10] restricts the discrete approximation to a fraction of the DCS. A cutoff angle, μ_{cut} can be defined, below which the continuous DCS is used. In the hybrid case, interaction cross sections are defined for elastic scattering above and below μ_{cut}. These are then implemented as separate interactions.

To compute these cross sections, we must first understand how the EEDL cross sections are normalised. The tabulated differential cross sections between -1 and μ_{SR} are normalised to unity,

$$\int_{-1}^{\mu_{SR}} \frac{d\sigma_{EEDL}(\mu, E)}{d\mu}\, d\mu = 1 \tag{4}$$

but the screened Rutherford portion,

$$\int_{\mu_{SR}}^{1} \frac{d\sigma_{SR}(\mu, E)}{d\mu}\, d\mu = \sigma_{SR}(E) \tag{5}$$

is normalised such that the analytical differential cross section is anchored to the data at $\mu = \mu_{SR}$, so $\sigma_{SR}(E) << 1$ at low energy and $>>$ 1 at high energy. The EEDL provides an interaction cross section for elastic scattering $\sigma_{el,cutoff}(E)$, but this cross section does not include the contribution from the screened Rutherford portion. The total electron elastic scattering can be calculated as the sum of the integrals over both parts of the differential cross section, multiplied by the cutoff cross section:

$$\sigma_{el,total} = \sigma_{el,cutoff}(E)\left(1 + \int_{\mu_{SR}}^{1} \frac{d\sigma_{SR}(\mu, E)}{d\mu}\, d\mu\right). \tag{6}$$

The fraction of the total cross section that lies above μ_{cut} is then

$$\frac{\sigma_{el,\ \mu>\mu_{cut}}}{\sigma_{el,total}} = \frac{\int_{\mu_{cut}}^{\mu_{SR}} \frac{d\sigma_{EEDL}(\mu, E)}{d\mu}\, d\mu + \int_{\mu_{SR}}^{1} \frac{d\sigma_{SR}(\mu, E)}{d\mu}\, d\mu}{1 + \int_{\mu_{SR}}^{1} \frac{d\sigma_{SR}(\mu, E)}{d\mu}\, d\mu} \tag{7}$$

and the fraction that lies below μ_{cut} is

$$\frac{\sigma_{el,\ \mu<\mu_{cut}}}{\sigma_{el,total}} = \frac{\int_{-1}^{\mu_{cut}} \frac{d\sigma_{EEDL}(\mu, E)}{d\mu}\, d\mu}{1 + \int_{\mu_{SR}}^{1} \frac{d\sigma_{SR}(\mu, E)}{d\mu}\, d\mu}. \tag{8}$$

The cross section for an interaction below μ_{cut}, $\sigma_{el,cont}$ which samples from the continuous DCS is then given by

$$\sigma_{el,cont} = \left[1 - \frac{\sigma_{el,>\mu_{cut}}}{\sigma_{el,total}}\right]\sigma_{el,total} \tag{9}$$

and the discrete cross section is

$$\sigma_{el,disc} = \left[1 - \frac{\sigma_{el,<\mu_{cut}}}{\sigma_{el,total}} - \alpha_0\right]\sigma_{el,total} \tag{10}$$

where α_0 is the weight of the $\mu = 1$, straight-ahead angle.

III. RESULTS

In this section, the full electron-photon transport physics is modelled in all Monte Carlo results. The GBFP is applied to the elastic scattering only and unless otherwise stated, the inelastic physics are handled using the analogue method.

1. 1D Energy Deposition Convergence

Figure 2 plots the energy deposition profile into a slab of silicon due to a 30 keV monoenergetic electron source and the associated error. The 1D TIGER geometry is used and 2×10^7 source particles are simulated to improve convergence in the low deposition region at the rear of the slab. To study the effect of varying μ_{cut}, the number of discrete angles is held constant and set to 1. For this problem, it is seen that the deposition profiles converge to the analogue result for increasing μ_{cut}. Table I shows the computational effort required using the GBFP method compared to analogue. Since the method is applied only to the elastic component of electron transport, both the average number of elastic scatters per history and the average time taken per history are shown. The reduction in the number of elastic scatters per history are in line with what would be expected for a 30 keV source with respect to the cross section reduction at this energy shown in Figure 1.

TABLE I: Computational speedups obtained by varying μ_{cut} with a single discrete angle above cutoff.

μ_{cut}	Avg. No. of Elastic Scatters per History	GBFP/Analogue	Avg. Time per History (sec)	GBFP/Analogue
Analogue	1093.45	-	0.09553	-
0.9	392.50	0.3590	0.07466	0.7815
0.5	241.42	0.2208	0.06878	0.7200
0.0	181.19	0.1657	0.06638	0.6948
-0.5	145.46	0.1330	0.06529	0.6834
-1.0	119.32	0.1091	0.06388	0.6687

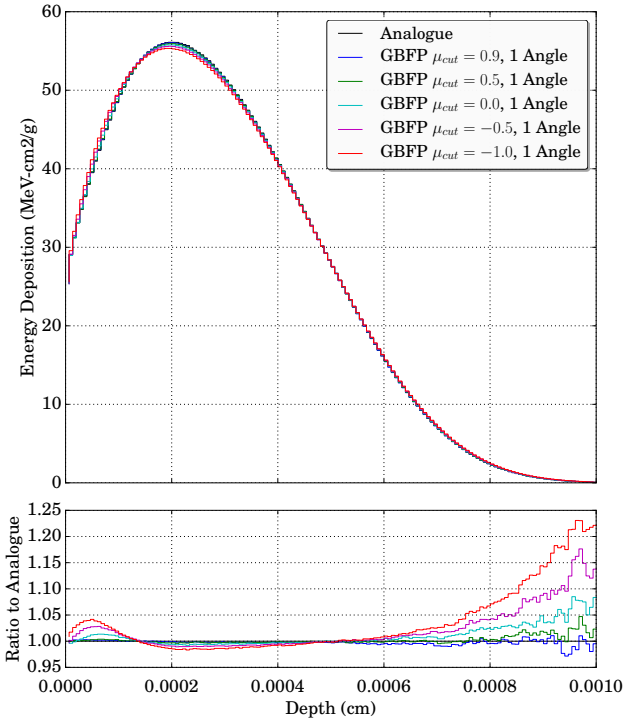

Fig. 2: Varying μ_{cut} for the 30 keV electrons into Silicon problem

2. 1D Comparison with Experiment

Figure 3 plots experimental data obtained by McLaughlin et al.[11] against the Monte Carlo results. The analogue results plotted are obtained using the LLNL cross sections. The GBFP curves are obtained with GBFP applied to the elastic scatter with analogue inelastic scatter, both using the LLNL data. 240000 particle histories were run in all cases. The condensed history curve is ITS in its default setting: condensed history for both elastic and inelastic scatter using the default cross section data. The experimental data sits roughly between the Monte Carlo results using the LLNL data and the ITS condensed history result. The experimental error was not published. The difference between the analogue and the GBFP result, even for a single discrete angle over the entire angle range is small in comparison to the difference between the analogue and both the experimental data and the ITS condensed history. The experimental response is greater than the numerical results at the rear side of the material. This is in agreement with what was observed by McLaughlin in his comparison with numerical results and is explained as being due to the dye film system used in the experiment.

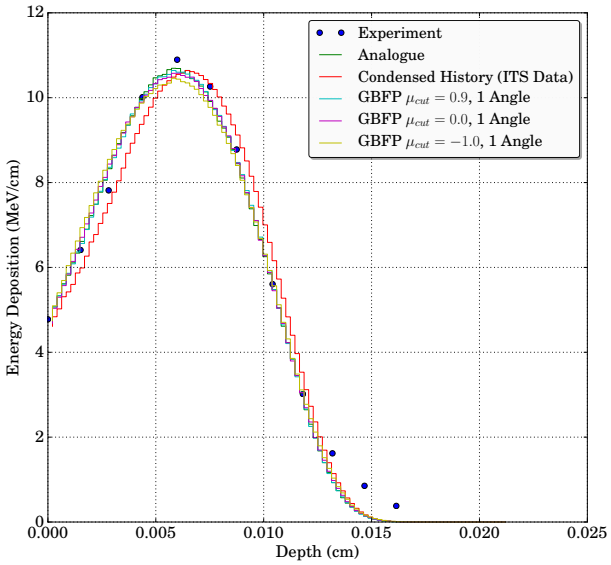

Fig. 3: 100 keV electrons into polystyrene. Experimental data vs. LLNL Analogue vs. LLNL GBFP vs. ITS Condensed History.

3. Angular Scattering Through Thin Foils

The results so far have presented quantities integrated in angle. One might expect these results to be less sensitive to changes to the elastic scattering method. Figure 4 plots the angular distribution of electrons escaping the rear of a 0.1 micron tantalum foil due to a 100 keV electron source at the front. In this problem, $\mu_{cut} = -1$ and the number of discrete angles is varied. 4.8×10^8 particle histories are run in all cases. Artefacts are clearly visible in the angular distribution corresponding to locations of the discrete angles. The amplitudes of these perturbations however decrease with the number of discrete angles, becoming almost indistinguishable from the analogue result at 8 angles. The ITS condensed history results suffer from errors at escape angles near $\mu = 0$. These were described

by Foote and Smyth[12] and are due to the angular scattering at the material boundaries imposed by the algorithm.

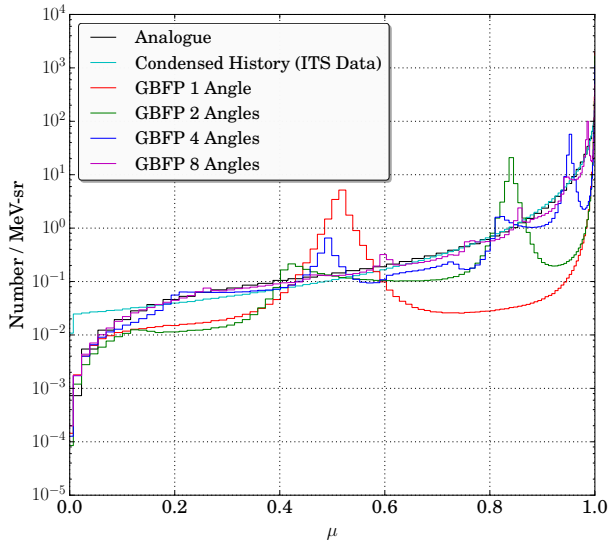

Fig. 4: Angular distribution of electrons emitted from the rear surface of a 0.1 micron tantalum foil with respect to the location of a 100 keV electron source.

Figures 5 and 6 plot the angular distributions of electrons escaping the rear and front surfaces of a 1 micron foil respectively. With this thicker target the artefacts in the angular distribution from the discrete angle approximation are significantly damped due to enough electrons having scattered elastically more than once. The GBFP results are indistinguishable from the analogue results using more than 2 discrete angles at the rear surface. At the front surface, the artefacts are more persistent, albeit with narrower peaks.

4. 2D Results

This problem measures the energy deposition distribution of a 300 keV electron source incident on a cylindrically symmetric slab of water using the CYLTRAN geometry in ITS. The energy deposition plots using the analogue method and the GBFP method using various combinations of μ_{cut} and number of discrete angles are shown in Figure 7. As with the results shown here previously, the GBFP method is applied to the elastic scattering only, with energy losses handled using the analogue method. Photon transport is enabled using the analogue method. Macroscopic EM fields are not simulated. 1×10^7 particles are run in all cases. In the case where a single scattering angle is used over the entire cosine range (Figure 7b), the spread of the deposition near the source is reduced, and there is noticeably less deposition close to the $z = 0$ axis. The GBFP results in Figures 7c and 7d are similar to the analogue result. Table II shows the average number of elastic scattering events that occur during a particle history using the GBFP method. While up to 100 fewer elastic scattering interactions are processed using the GBFP method compared

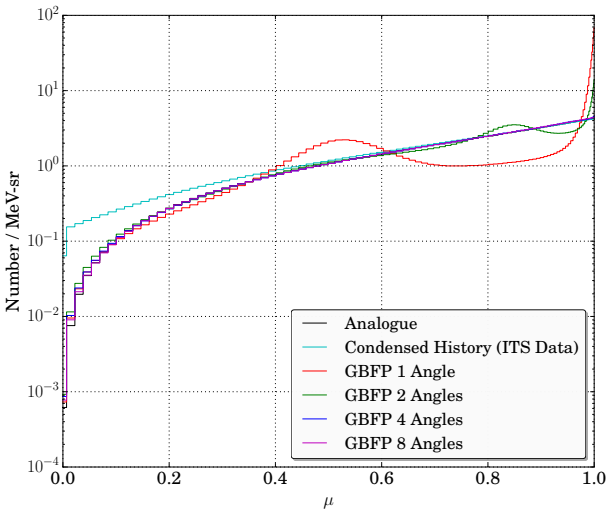

Fig. 5: Angular distribution of electrons emitted from the rear surface of a 1 micron tantalum foil with respect to the location of a 100 keV electron source.

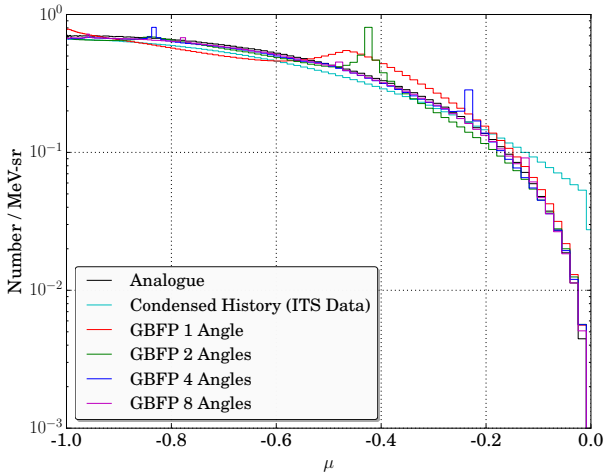

Fig. 6: Angular distribution of electrons emitted from the front surface of a 1 micron tantalum foil with respect to the location of a 100 keV electron source.

to analogue, this is not manifested to the same extent in the average compute time per particle (Table III). Once again, this highlights a need to extend this method to the inelastic physics.

The ratios of the GBFP results to the analogue results integrated around the cylindrical volume as a function of radius and depth are shown in Figure 8. The results shown are not normalised by volume and are binned uniformly in radius (ρ). The cells at greater radii therefore correspond to an integration over a larger volume. Figure 8b plots the worst case results for the GBFP method: a single discrete angle over the entire cosine range. Artefacts of the method are clearly visible in this case, with the GBFP method overestimating the deposition in the line of sight of the source by more than a factor of

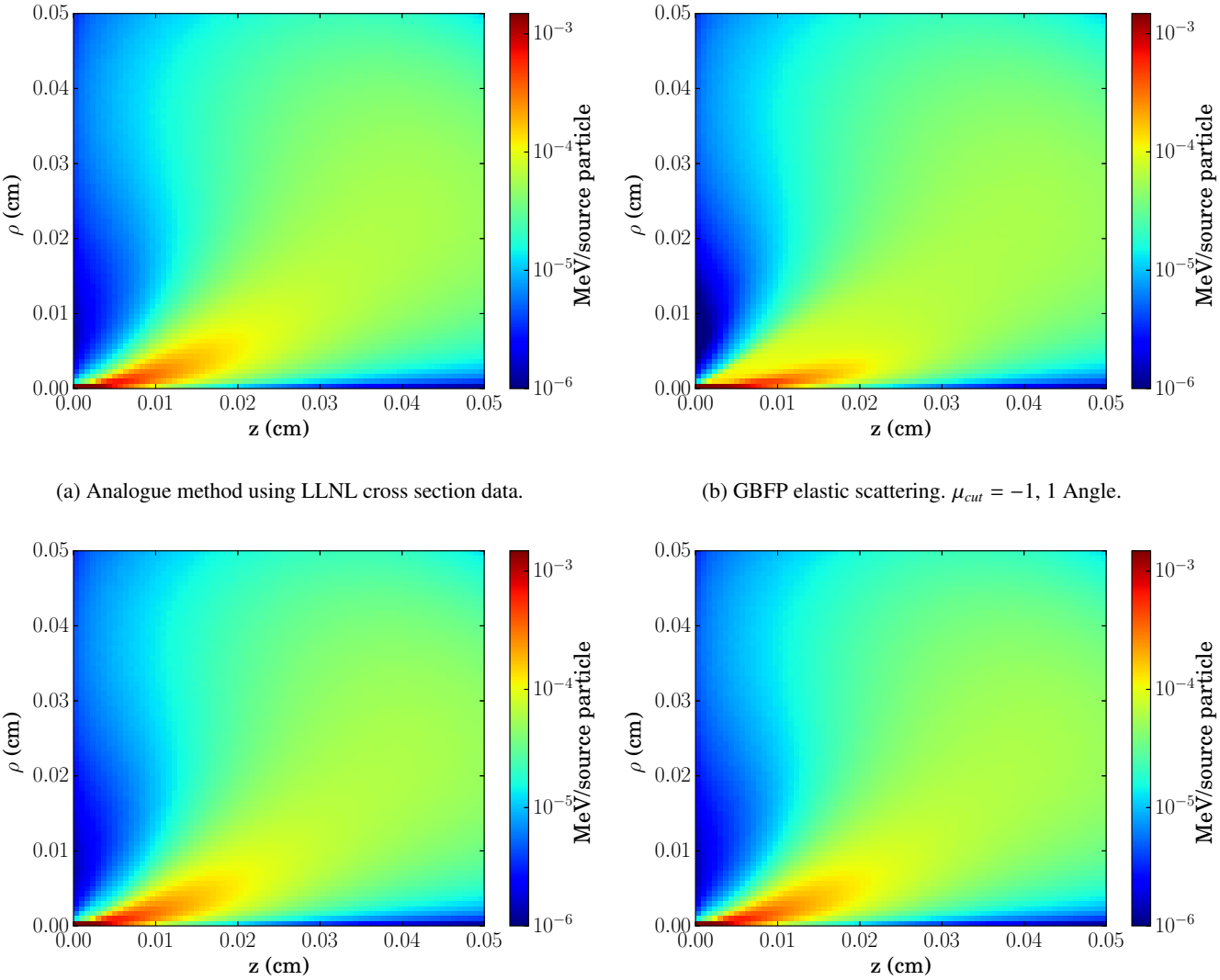

(a) Analogue method using LLNL cross section data.

(b) GBFP elastic scattering. $\mu_{cut} = -1$, 1 Angle.

(c) GBFP elastic scattering. $\mu_{cut} = -1$, 4 Angles.

(d) GBFP elastic scatting. $\mu_{cut} = 0.9$, 1 Angle.

Fig. 7: Energy deposition in a 2D slab of water due to a 300 keV electron source at (0,0) emitting in the positive z direction. Figure (a) plots the analogue results. Figures (b-d) plot the results using the GBFP method for elastic scattering with analogue inelastic scattering.

2.7, and underestimating the deposition in the regions away from the discrete angle by around a factor of 2. In Figure 8c, 4 discrete angles are used over the entire cosine range. While the ray effects are still visible close to the source, the amplitude of the rays is substantially decreased in comparison to the single angle case in 8b, with the overestimation in the rays being below 1.2 times the analogue result, and 0.84 times the analogue result outside the rays. In Figure 8d the discrete angle cutoff, μ_{cut} is increased to 0.9 with a single discrete angle between μ_{cut} and 1. The ray effects here are faintly visible near the source. In this case the greatest and smallest ratio is actually found down the $z = 0$ axis and is around 10%, although statistical error is likely to be responsible for these extreme values. The GBFP results are all seen to agree with the analogue result at a radius of $0.045cm$ into the material.

The default ITS code is compared with the analogue results in Figure 8a. To clarify, the default ITS code uses a condensed history method, using cross section data from NIST supplemented with built in physics models. The analogue method refers to the single-scattering algorithm implemented using only cross section data from the EEDL, EADL and EPDL data libraries from LLNL. The largest difference is seen in the straight-ahead direction from the source at a distance corresponding to the condensed history substep size. The default substep size for 300 keV electrons in water is 0.0025825 cm. Error persists in the simulation as an artefact from the first

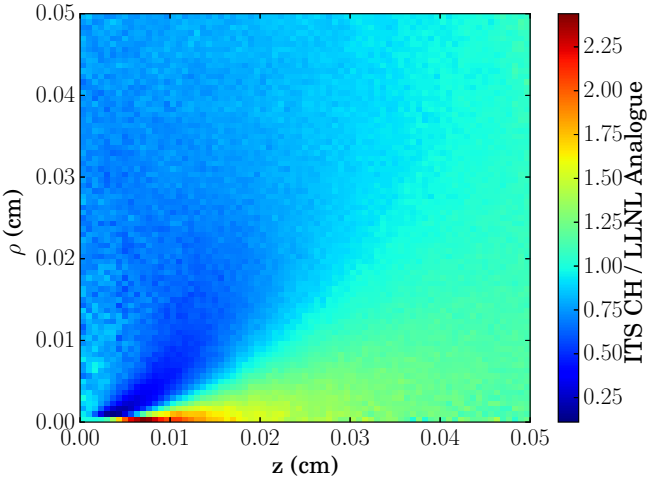

(a) Default ITS Condensed History / Analogue with LLNL cross sections

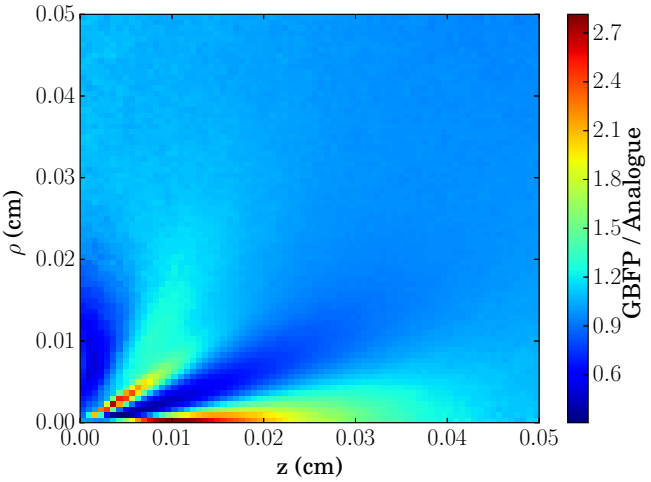

(b) GBFP/Analogue. $\mu_{cut} = -1$, 1 Angle.

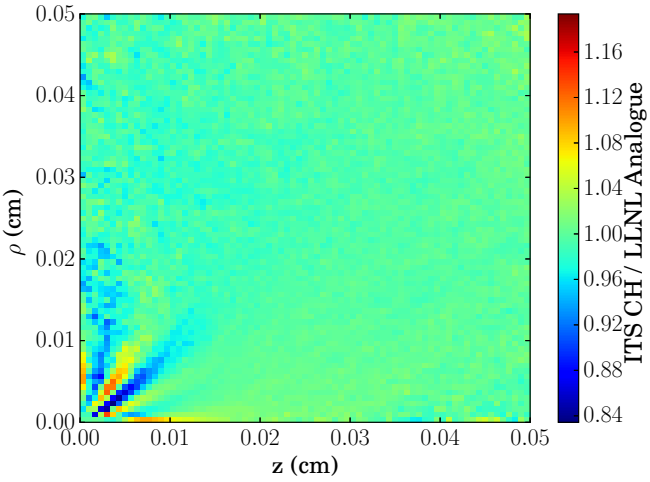

(c) GBFP/Analogue. $\mu_{cut} = -1$, 4 Angles.

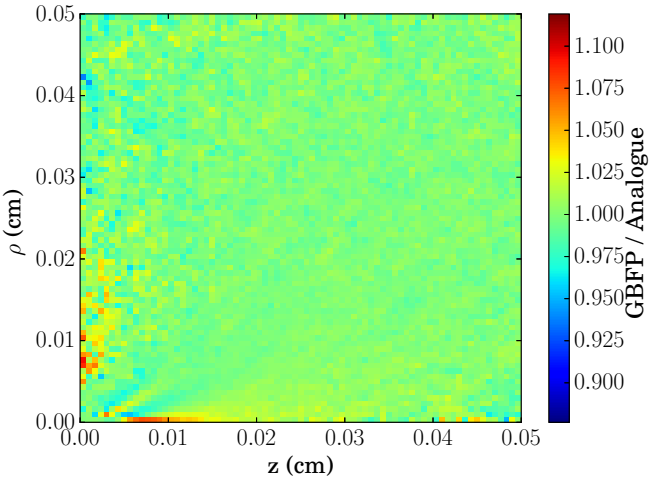

(d) GBFP/Analogue. $\mu_{cut} = 0.9$, 1 Angle.

Fig. 8: Figures (b-d) plot the ratio of GBFP results shown in Figure 7 to the analogue result for energy deposition in a 2D slab of water due to a 300 keV electron source at (0,0) emitting in the positive z direction. The ratio of the default ITS method and cross sections to the analogue method with LLNL cross sections is plotted in (a).

substep over which the electron only moves in the z direction and scatters in angle at the end of the substep. The dose is over-estimated along the z-axis and is greatest at depths of 2-3 substeps. The dose is underestimated at small radii at depths from 0.5-2 substeps due to the delay in the angular scattering. These artefacts could be reduced by decreasing the substep size in the condensed history algorithm. However, since there is currently no facility in ITS to run an analogue simulation using the NIST data, it is not clear to what extent the differences are due to the condensed history method, rather than differences in the cross section data.

IV. SUMMARY

The GBFP method has been applied to produce an approximate elastic differential cross section from the tabulated data in the Evaluated Electron Data Library. The method has been shown to converge to the analogue result with increasing μ_{cut} for the energy deposition problem, and was shown to offer up to an order of magnitude decrease in the number of elastic scattering events for a 30keV electron source. For the 300 keV electron source problem, this speedup was seen to be even larger. The effect of the discrete representation on quantities differential in angle was demonstrated, with artefacts visible

TABLE II: The average number of elastic scattering events processed per history using GBFP method for the 300 keV electrons into water problem.

μ_{cut}	Number of Discrete Angles			
	1	2	4	Analogue
-1.0	24.00	58.99	139.21	-
0.0	37.81	91.02	208.59	-
0.9	169.27	351.89	558.87	-
Analogue	-	-	-	2409.33

TABLE III: The average compute time per history (in seconds) using the GBFP method for the 300 keV electrons into water problem.

μ_{cut}	Number of Discrete Angles			
	1	2	4	Analogue
-1.0	0.469	0.474	0.479	-
0.0	0.472	0.476	0.486	-
0.9	0.481	0.492	0.513	-
Analogue	-	-	-	0.592

in thin films which are attenuated with increasing thickness. In 2D, ray effects were visible near the source for an electron beam problem. These effects however are seen to be alleviated with increasing both the number of discrete angles and μ_{cut}.

The computational speedups presented here (Tables I and II) are expressed in terms of the reduction in the number of elastic scattering events that are required to be processed by the method. This does not account for the time taken to process the inelastic physics. No biasing has been applied to any of the simulations. The implementation of the electron trapping (or range rejection) biasing mechanism will also significantly improve runtimes. The EADL contains detailed atomic ionisation and relaxation data which is implemented currently using an analogue scattering algorithm. To realise the significant runtime improvements implied by the reduction in the number of elastic scattering events that require processing due to the GBFP treatment, a moment preserving method for inelastic processes is essential.

V. ACKNOWLEDGMENTS

Sandia is a multi-mission laboratory operated by Sandia Corporation, a Lockheed Martin Company, for the United States Department of Energy's National Nuclear Security Administration under Contract DE-AC04-94AL85000.

REFERENCES

1. B. FRANKE, R. KENSEK, T. LAUB, and M. CRAWFORD, "ITS Version 6: The Integrated TIGER Series of Coupled Electron/Photon Monte Carlo Transport Codes," Tech. Rep. SAND2008-3331, Sandia National Laboratories (2009).
2. S. PERKINS and D. CULLEN, "ENDL type formats for Evaluated Atomic Library, EADL, for the Evaluated Electron Library, EEDL and for the Evaluated Photon Data Library, EPDL," *UCRL-ID-117796* (1994).
3. B. FRANKE and A. PRINJA, "Monte Carlo Electron Dose Calculations Using Discrete Scattering Angles and Discrete Energy Losses," *Nuc. Sci. Eng.*, **149**, 1–22 (2005).
4. D. DIXON, A. PRINJA, and B. FRANKE, "A Computationally Efficient Moment-Preserving Monte Carlo Electron Transport Method with Implementation in GEANT4," *Nuc. Inst. Meth. B*, **359**, 20–35 (2015).
5. B. FRANKE, R. KENSEK, and A. PRINJA, "Evaluation of Monte Carlo Electron-Transport Algorithms in the Integrated Tiger Series Codes for Stochastic-Media Simulations," *Joint International Conference on Supercomputing in Nuclear Applications and Monte Carlo* (2013).
6. S. SELTZER, "An Overview of ETRAN Monte Carlo Methods," in T. JENKINS, W. NELSON, and A. RINDI, editors, "Monte Carlo Transport of Electrons and Photons," Plenum Press, New York, pp. 153–181 (1988).
7. L. V. SPENCER, "Theory of Electron Penetration," *Phys. Rev.*, **98**, 1597 (1955).
8. D. P. SLOAN, "A New Multigroup Monte Carlo Scattering Algorithm for Neutron and Charged-Particle Boltzmann and Fokker-Planck Calculations," Tech. Rep. SAND83-7094, Sandia National Laboratories (1983).
9. J. E. MOREL, L. J. LORENCE, R. P. KENSEK, J. A. HALBEIB, and D. P. SLOAN, "A Hybrid Multigroup/Continuous Energy Monte Carlo Method for Solving the Boltzmann-Fokker-Planck Equation," *Nuc. Sci. Eng.*, **124**, 369 (1996).
10. B. FRANKE, A. PRINJA, and L. HARDING, "Monte Carlo Electron Transport Using Generalized Boltzmann Fokker-Planck Scattering Models," *Mathematics and Computation, Supercomputing, Reactor Physics and Nuclear and Biological Applications* (2005).
11. W. L. MCLAUGHLIN and E. K. HUSSMAN, "The Measurement of Electron and Gamma-Ray Dose Distributions in Various Media," in "Large Radiation Sources for Industrial Processes," IAEA, IAEA-SM-123/43.
12. B. FOOTE and V. SMYTH, "The modelling of electron multiple scattering in EGS4/PRESTA and its effect on ionisation chamber response," *Nuc. Inst. Meth. B*, **100**, 30 (2005).